




Motor Unit Magnetic Resonance Imaging (MUMRI) In Skeletal Muscle

Linda Heskamp,^{1,2*}  Matthew G. Birkbeck,^{1,3,4*}  Daniel Baxter-Beard,¹ Julie Hall,^{1,5} Ian. S. Schofield,¹ Mathew Elameer,^{1,5} Roger G. Whittaker,^{1,6} and Andrew M. Blamire¹ 

Magnetic resonance imaging (MRI) is routinely used in the musculoskeletal system to measure skeletal muscle structure and pathology in health and disease. Recently, it has been shown that MRI also has promise for detecting the functional changes, which occur in muscles, commonly associated with a range of neuromuscular disorders. This review focuses on novel adaptations of MRI, which can detect the activity of the functional sub-units of skeletal muscle, the motor units, referred to as “motor unit MRI (MUMRI).” MUMRI utilizes pulsed gradient spin echo, pulsed gradient stimulated echo and phase contrast MRI sequences and has, so far, been used to investigate spontaneous motor unit activity (fasciculation) and used in combination with electrical nerve stimulation to study motor unit morphology and muscle twitch dynamics. Through detection of disease driven changes in motor unit activity, MUMRI shows promise as a tool to aid in both earlier diagnosis of neuromuscular disorders and to help in furthering our understanding of the underlying mechanisms, which proceed gross structural and anatomical changes within diseased muscle. Here, we summarize evidence for the use of MUMRI in neuromuscular disorders and discuss what future research is required to translate MUMRI toward clinical practice.

Level of Evidence: 5

Technical Efficacy: Stage 3

J. MAGN. RESON. IMAGING 2024.

Around 14 million people are affected by neuromuscular disease worldwide.¹ Symptoms typically comprise weakness, fatigue, and muscle pain and clinical signs like muscle wasting, increased levels of spontaneous muscle activity (fasciculation) and tendon reflex hypoactivity or hyperactivity. The basic constituent of the neuromuscular system is the motor unit; a single motor nerve axon with cell body in the spinal cord anterior horn, which divides within the muscle to supply multiple skeletal muscle fibers (Fig. 1). The number of fibers within a motor unit varies within and between muscles; from as few as 10 muscle fibers for motor

units of small muscles like extraocular muscles to several hundred in large postural muscles like the quadriceps and glutei. Muscle fibers within a motor unit are widely spaced, therefore fibers from neighboring units interdigitate and overlap each other.^{2,3}

The most fundamental role of the motor unit is to generate movement. A single action potential in the motor nerve fiber results in the coordinated contraction of each of the muscle fibers within the supplied motor unit. The force generated is transmitted to the joint via the intramuscular connective tissue and muscular tendon, to produce a muscle

View this article online at [wileyonlinelibrary.com](https://onlinelibrary.wiley.com/doi/10.1002/jmri.29218). DOI: 10.1002/jmri.29218

Received Aug 9, 2023, Accepted for publication Dec 20, 2023.

*Address reprint requests to: L.H., Newcastle University Translational and Clinical Research Institute (NUTCRI), Newcastle University, Newcastle upon Tyne, United Kingdom; Department of Radiology, University Medical Centre Utrecht, Utrecht, The Netherlands. E-mail: linda.heskamp@newcastle.ac.uk; l.heskamp-2@umcutrecht.nl, or M.B., Newcastle University Translational and Clinical Research Institute (NUTCRI), Newcastle University; Newcastle Biomedical Research Centre (BRC), Newcastle University; Northern Medical Physics and Clinical Engineering, Freeman Hospital, Newcastle upon Tyne NHS Foundation Trust, Newcastle upon Tyne, UK. E-mail: matt.birkbeck@newcastle.ac.uk

The last two authors are Joint senior authors.

From the ¹Newcastle University Translational and Clinical Research Institute (NUTCRI), Newcastle University, Newcastle Upon Tyne, UK; ²Department of Radiology, University Medical Centre Utrecht, Utrecht, The Netherlands; ³Newcastle Biomedical Research Centre (BRC), Newcastle University, Newcastle upon Tyne, UK; ⁴Northern Medical Physics and Clinical Engineering, Freeman Hospital, Newcastle upon Tyne NHS Foundation Trust, Newcastle upon Tyne, UK; ⁵Department of Neuroradiology, Royal Victoria Infirmary, Newcastle upon Tyne NHS Foundation Trust, Newcastle upon Tyne, UK; and ⁶Directorate of Clinical Neurosciences, Royal Victoria Infirmary, Newcastle upon Tyne NHS Foundation Trust, Newcastle upon Tyne, UK

Additional supporting information may be found in the online version of this article

This is an open access article under the terms of the [Creative Commons Attribution](https://creativecommons.org/licenses/by/4.0/) License, which permits use, distribution and reproduction in any medium, provided the original work is properly cited.

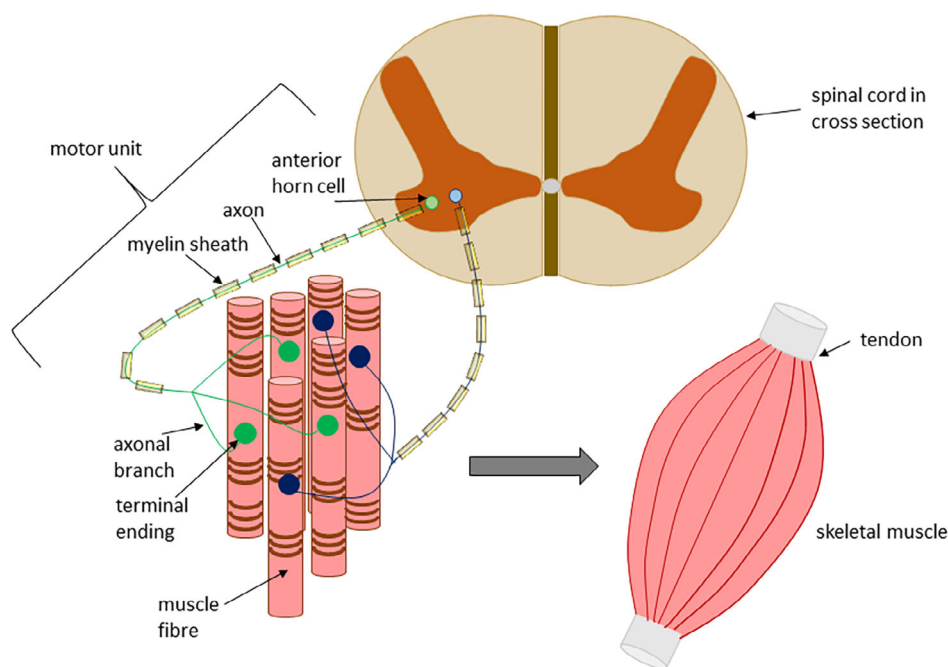


FIGURE 1: Schematic representation of motor unit and muscle. Schematic shows spinal cord in cross section with two motor units (one in green and the other in blue) shown constituent of: anterior horn cell in the spinal cord, myelinated axon, and the constituent muscle fibers belonging to that motor unit. Motor units are interdigitated within skeletal muscle. Multiple motor units make up a single skeletal muscle which is shown inserting to the tendon.

twitch lasting between ~ 200 and 300 msec.⁴ As the frequency of action potentials increases, these single twitches fuse to generate a steady tension at the joint. Motor units rarely act in isolation and a voluntary movement typically involves coordinated activity in multiple overlapping units with an increase in force modulated both by recruitment of larger units and by increasing their firing frequency (i.e., number of times the motor unit activates in a given time period).⁵

Neuromuscular diseases disrupt both motor unit structure and function. In primary muscle diseases such as myositis, the number of motor units remains essentially unchanged, but muscle fibers within a given unit show both atrophy and compensatory hypertrophy.⁶ Consequently, the force generated by individual motor units decreases and increased numbers of units must then be recruited for a given strength of voluntary movement. In contrast, diseases primarily affecting the motor nerve, such as polio and spinal muscular atrophy (SMA), result in a reduced number of motor units, each of which contain an increased number of fibers.⁷ Hyperexcitability of the motor nerve results in spontaneous motor unit contraction or “fasciculation,” which can be visible in superficial muscles but is invisible in deeper muscles.

Various neurophysiological techniques, including nerve conduction studies, surface electromyography (EMG) and needle EMG can study motor unit function.⁸ These have the advantage of low cost, excellent temporal resolution, and objective measurement of neuromuscular function. However, they can be painful, time-consuming, invasive, and in general have very poor spatial resolution. Increasingly, muscle

imaging is being used alongside neurophysiology to provide a more complete view of muscle pathophysiology. For example, magnetic resonance imaging (MRI) provides detailed images of muscle tissue anatomy, and can provide quantitative estimates of muscle metabolites, edema and fat replacement not visible using neurophysiological techniques, and with excellent spatial resolution.^{9,10}

The fundamental limitation of current muscle MRI is that although it provides detailed information on muscle *structure*, images are static and provide no indication of muscle *function*. Clinically, this poses a particular challenge because muscle fat replacement usually occurs as the disease’s end-stage, representing permanent contractile muscle tissue loss. Changes in T_2 -weighted \pm short tau inversion recovery (STIR) sequences differ between populations with established motor nerve disorders and healthy controls, and within diseased cohorts changes can be observed longitudinally. A link has been proposed between T_2 -weighted signal change and loss of motor neurons, although further research is required to confirm this.¹¹ However, at the individual level, T_2 -weighted signal changes do not always reflect the clinical or neurophysiological status of disease. Furthermore, at least for auto-immune myopathy, STIR signal can be normal in regions with biopsy proven inflammation.¹² For many diseases, but particularly chronic or progressive muscle and nerve disorders, functional changes can precede structural changes. Methods to detect these functional changes could facilitate earlier diagnosis and offer more accurate disease biomarkers essential to the future management of these conditions.

Recent work has demonstrated that MRI can be used to image the muscle fibers contraction and relaxation associated with motor unit activation and therefore further expands the potential of MRI to research and diagnose neuromuscular diseases. In this review, we discuss the emerging field of motor unit MRI (MUMRI), considering the historical and technical background and supporting evidence for use of MRI in this context and illustrate the emerging clinical applications for this technique.

Historical Observations

The first evidence that MRI was sensitive to the functional activity of discrete motor units emerged from studies applying diffusion weighted imaging (DWI) sequences to investigate muscle microstructure, although the connection to the potential clinical value of the observations was not immediately recognized. The uses of sequences such as DWI, where motion-encoding gradients are employed to characterize molecular motion of water are also intrinsically sensitive to the bulk motion of muscle fibers. Early work, such as by Lemberskiy et al.¹³ reported the presence of sporadic and spontaneous signal voids on diffusion weighted (DW) muscle images, which at the time were considered an inconvenient, but unexplained artifact (Fig. 2). Subsequent work by Steidle et al.¹⁴ concluded that these regional signal voids arose from “spontaneous mechanical activities of musculature” (SMAMs). Imaging in these studies has typically used diffusion b -values of 100 to 500 sec/mm² while the observed signal

attenuation has been by more than 80%, much greater than could be attributed to diffusion processes alone. Szevenyi et al.¹⁵ then proposed the link between SMAMs and the recognized physiological process of motor unit fasciculation, which has led to the evolution of MUMRI methods. This link with motor unit activity was further confirmed by Whittaker et al.¹⁶ who combined a DWI sequence with controlled electrical stimulation of motor units in the lower legs of healthy controls. Based on these observations they named the technique motor unit MRI (MUMRI).

Technical Background to Motor Unit MRI

Two main types of sequence have been used to detect and report on different features of motor unit activity. DWI sequences are used to image the distribution and spatial extent of motor unit activity, and phase contrast (PC) sequences to measure the velocity of moving muscle tissue and with this the twitch dynamics of whole muscles and single motor units. Since motor unit firing is a dynamic process, both sequences make use of an echo-planar imaging (EPI) read-out to allow single-shot dynamic imaging.

Single Shot DW Sequences

Originally, DW sequences were designed to detect the diffusive (Brownian) motion of water molecules in tissue. In conventional clinical application they are used to detect areas of restricted diffusion e.g. to image infarcted tissue in the central nervous system following stroke.¹⁷ However, any process which re-arranges the *relative* spatial position of water molecules within the imaging voxel will produce a signal attenuation. One such mechanism within muscle tissue is muscle fiber contraction and relaxation within motor units. Therefore, if a motor unit fires and muscle tissue movement occurs within the sequence’s motion-sensitive time period (Δ), localized signal attenuation will be visible in the image at the location of muscle contraction (Fig. 2). The sensitivity of the sequence to water molecule reordering is determined by the sequence b -value. The underlying explanation for this contrast is discussed in more detail in section “[Explanation of the contrast mechanism in single shot DW MUMRI.](#)” First, we will discuss the two different types of motion preparation, the pulsed gradient spin echo (PGSE) and pulsed gradient stimulated echo (PGSTE). Each method has advantages and drawbacks in the MUMRI context. It is particularly important to note that while these methods are commonly referred to in conventional use as DW sequences; the contrast mechanism for MUMRI is intravoxel contraction of tissue and not diffusion.

The PGSE sequence employs two identical motion-sensitizing gradients on either side of the 180° radiofrequency (RF) refocusing pulse (Fig. 3a). In comparison the PGSTE sequence employs three 90° RF pulses, in which the second 90° RF pulse tips the magnetization into the longitudinal axis (Fig. 3b). As a result, the magnetization does not experience T_2

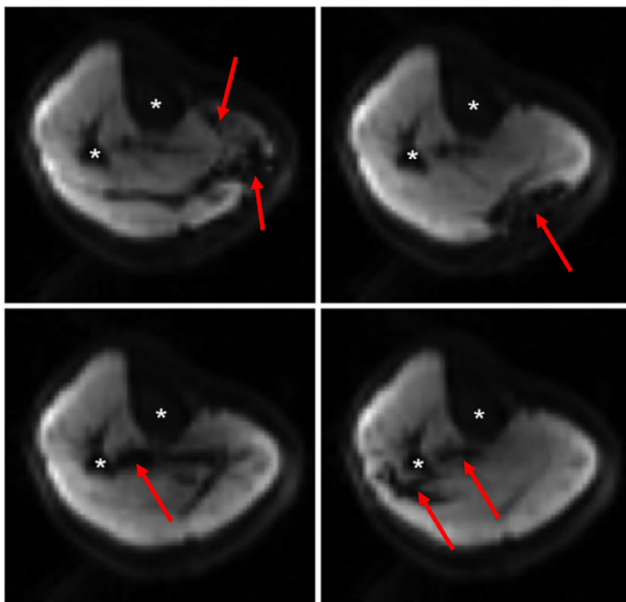


FIGURE 2: Typical examples of short-lived signal voids in transverse images of the resting low leg of a 33-year old healthy participant recorded by a single shot PGSTE sequence. Regions with pronounced signal voids are clearly visible in the soleus, gastrocnemius, and tibialis posterior muscles, indicated by the red arrows. Areas with low signal intensity due to bone (tibia and fibula) are highlighted by the white asterisks. Figure re-used with permission from Steidle et al.¹⁴

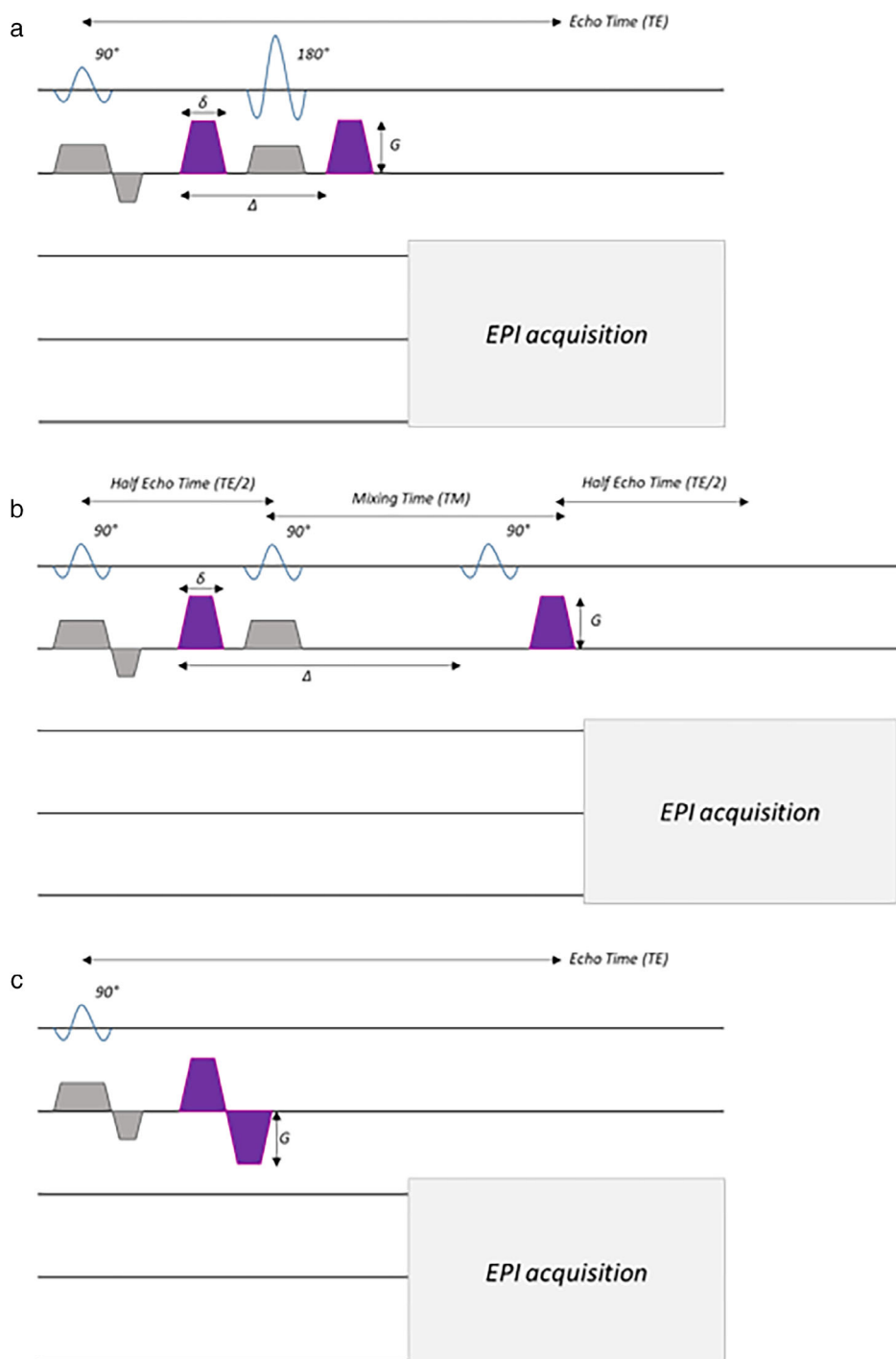


FIGURE 3: Pulse sequence diagrams. (a) Single shot pulsed gradient spin echo (PGSE) sequence. (b) Single shot PGSTE sequence. (c) PC sequence. In (a,b), the motion-sensitive gradients are indicated in purple and the motion-sensitization times (δ/Δ) and gradient strength (G) are indicated by the black arrows. In (c), velocity encoding gradients are displayed in purple. They could be applied in any direction, for simplicity here shown only along the slice encoding direction. The diagram includes the echo planar readout module used in most publications.

relaxation during the mixing time (TM), instead only the much slower T_1 relaxation process occurs. The third 90° RF pulse tips the magnetization back into the transverse plane to perform the measurement. The first motion-sensitization gradient is placed after the first 90° RF pulse and the second motion-sensitization gradient is placed after the third 90° RF pulse.

The PGSE sequence has the advantage of an inherently higher signal to noise ratio (SNR) compared to the PGSTE sequence.^{17–19} This is because the three 90° RF pulses in the PGSTE sequence return half of the excited magnetization to the longitudinal axis before signal readout, leading to 50% signal loss. The PGSTE sequence, however, allows exploration of

longer motion-sensitization times, because the TM interval can be lengthened without increasing the echo time (TE). As such, PGSTE avoids signal loss due to T_2 relaxation during most of the motion sensitive (TM) period. This is especially relevant in tissues with short T_2 water relaxation times, like skeletal muscle (T_2 water ≈ 30 msec²⁰). Consequently, in conditions where one aims to measure muscle with long sensitization times, the SNR of a PGSTE sequence can be higher than the SNR of a PGSE sequence.

Both PGSE and PGSTE sequences have been used for MUMRI in skeletal muscle. Only a single study has compared PGSTE and PGSE at different motion-sensitization times (Δ ; PGSTE: 100, 150, 200, and 250 msec; PGSE: 17 msec).¹⁸ That study demonstrated that the number of detected spontaneous muscle contractions increased with longer motion-sensitization periods (larger Δ values). However, this work was limited to lower leg imaging of only three healthy controls. The optimal choice of sequence will likely depend on the application, the required motion-sensitization time and the scanner's capabilities.

Explanation of the Contrast Mechanism in Single Shot DW MUMRI

Various studies investigated the underlying contrast mechanisms in PGSE and PGSTE images of skeletal muscle to prove that the short-lived localized signal voids are indeed resulting from muscle motor unit contraction. The first systematic proof was delivered by Steidle and Schick¹⁴ who applied a PGSTE sequence with a long motion-sensitization time ($\Delta = 145$ msec) and b -value of 100 sec/mm^2 to study spontaneous signal changes (Fig. 2). They excluded blood pulsation and subject positioning (prone vs. supine) as potential causes for the observed signal voids in skeletal muscle. Furthermore, based on repetitive imaging at different repetition times (TR), they concluded that the mechanism causing these signal voids has a time profile slightly longer than 200 msec, similar to an average muscle twitch time profile ($\sim 200\text{--}300$ msec).⁴ Other potential causes were discussed, including short-term and localized reduction in proton density, or shortening of T_1 or T_2 relaxation time. However, from a physiological point-of-view those are extremely unlikely. Therefore, they concluded that the only remaining explanation was microscopic incoherent mechanical activity of substructures within the muscle tissue, i.e., spontaneous contraction of muscle tissue.

Further proof was delivered when PGSTE imaging in resting muscle was combined with in-scanner EMG measurements. In 2018, Schwartz et al.¹⁹ used an MRI compatible surface EMG (sEMG) system and correlated the signal voids observed in the images with sEMG activity. The two measures were highly correlated, and the sEMG activity appeared before the signal void in the image (as expected since sEMG

detects the electrical change preceding the mechanical contraction). In the same study, sEMG activity was measured outside the scanner room, inside the scanner bore without scanning and during MR scanning. The EMG activity did not differ between the three conditions, suggesting that spontaneous muscle contraction is not induced by gradient switching, although a systematic study with more power will be needed to confirm this. Later, in-scanner sEMG measurements were used to trigger the MR sequence²¹ allowing synchronization of the image capture to EMG events. All images acquired following the trigger presented with signal voids near the EMG electrodes, while non-triggered images showed no signal voids. Furthermore, they showed that the time-profile of the mechanism causing the short-lived localized signal voids aligned with muscle twitch time-profiles (Fig. 4a–c).^{4,22}

Standard neurophysiological studies of skeletal muscle use surface electrical stimulation of innervating nerves to purposely activate motor units. Combination of nerve stimulation with synchronized imaging offers the opportunity to control and systematically dissect the contrast mechanism. Heskamp et al.²² performed a numerical simulation study that stepped the PGSE encoding gradients across a simulated muscle twitch profile and calculated the MR signal at each step. The resultant MR signal over time displayed two distinct signal attenuations, the first one resulting from the twitch contraction and the second one from the twitch relaxation. These simulations were compared to experimental data, in which the peroneal or tibial nerve was electrically stimulated and the lower leg imaged with a PGSE sequence ($b = 20 \text{ sec/mm}^2$). The timing of each nerve stimulation pulse was systematically varied in relation to the motion-sensitive gradients to map muscle twitch characteristics. The measured signal over time displayed the same two successive signal attenuations (Fig. 4c).

PC Sequence

The PC sequence employs a bipolar velocity encoding gradient after the RF excitation pulse to encode velocity information about the moving water (Fig. 3c). It is most commonly used clinically in cardiac MRI to measure blood flow velocities.²³ In MUMRI, it can be used to measure the bulk velocity of moving muscle tissue during muscle fiber contraction and relaxation.

The action of the gradients introduces a phase shift, which depends on the velocity with which the tissue water molecules are moving. The acquisition is repeated with the bipolar gradient in opposite polarity to calculate the velocity. It is important to note that the use of phase shifts is subject to the Nyquist criterion (phase evolution cannot exceed 180° during the sensitization), which means there is an upper limit on the detectable maximum velocity; the user must select a velocity encoding (VENC) value which is

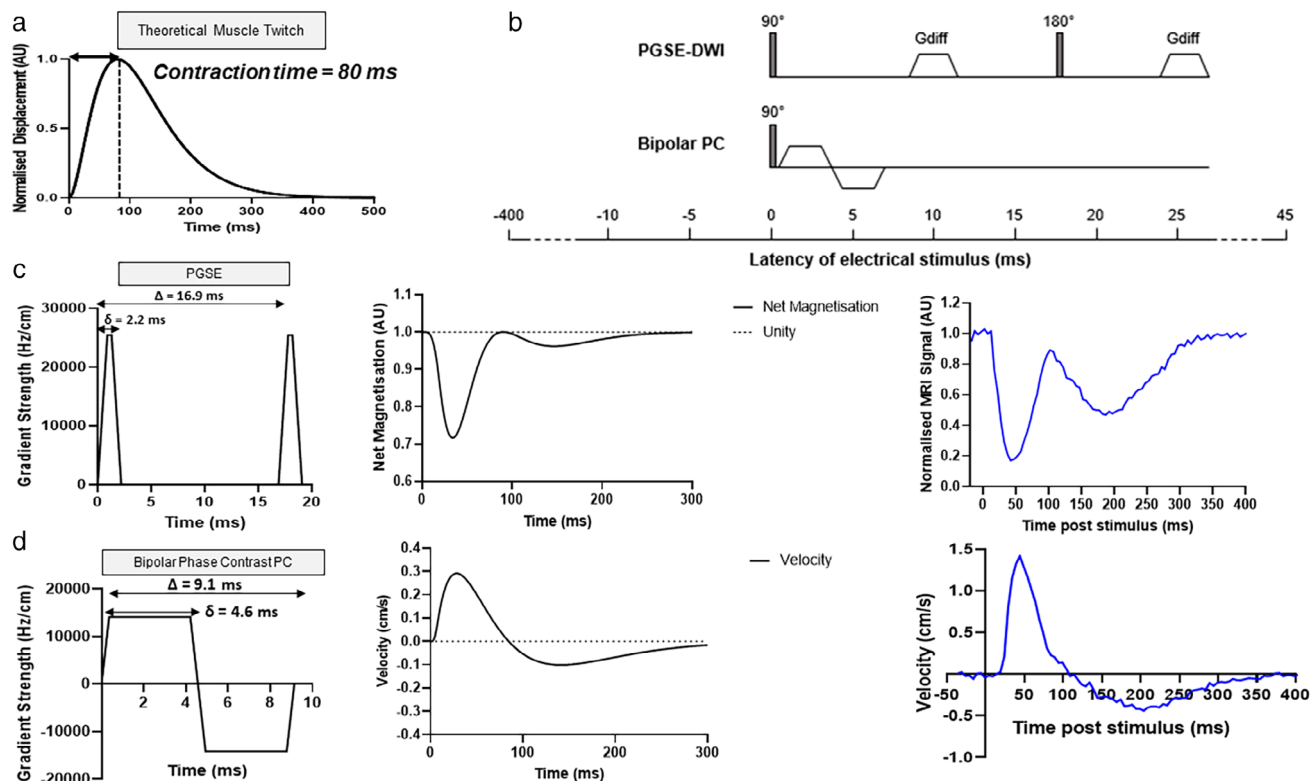


FIGURE 4: Example of a simulated MRI signal from a theoretical twitch profile and real-time example of the MRI signal in electrically stimulated muscle for the pulsed gradient spin echo (PGSE) sequence and PC sequence. (a) Simulated muscle twitch with a contraction time of 80 msec. (b) Schematic representation of the gradient waveforms for the PGSE and PC sequence and the timing of the electrical stimulus relative to the 90° radiofrequency pulse. (c) Left: The simulated PGSE gradient waveform that was stepped over the simulated twitch time-profile, showing the representative δ and Δ values. Middle: The resulting simulated MRI signal behavior demonstrating two consecutive signal drops, corresponding to the contraction and relaxation phase respectively. Right: Example of a real-world MRI signal from the tibialis anterior muscle during peroneal nerve stimulation in a healthy volunteer. This experimentally measured signal demonstrates two successive signal drops, as observed for the simulated signal (in middle). (d) Left: The simulated PC gradient waveform that was stepped over the simulated twitch time-profile, showing the representative δ and Δ values. Middle: The resultant velocity profile demonstrating a positive lobe (contraction) followed by a negative lobe (relaxation) before returning to baseline. Right: An example of a real-world velocity profile of single motor unit in the anterior compartment of the lower leg during peroneal nerve stimulation in a healthy volunteer. This experimentally measured signal demonstrates the positive and negative lobe, as observed for the simulated signal (in middle). Figure adapted from Heskamp et al.²²

appropriate for the tissue velocity to avoid signal aliasing. For recommended VENC values, see section “[Imaging of motor unit twitch profile.](#)”

Simulations of muscle fiber contraction for a PC sequence demonstrated that stepping the bi-polar gradient across the simulated muscle twitch resulted in a phase signal with initially a positive lobe (representing contraction) and a negative lobe (representing relaxation) (Fig. 4b,d). This signal behavior was also reported for experimentally obtained PC images during electrical stimulation of the lower leg’s anterior muscle compartment. It is important to note the difference in the two mechanisms, which give rise to change in contrast. For a PC sequence, it is the overall bulk movement of water in muscle tissue along the direction in which the velocity encoding gradients are applied. For the PGSE/PGSTE sequences, it is the incoherent re-ordering of the water molecules, which causes signal attenuation and the overall bulk movement of water is less relevant.

Single Shot DW Imaging vs. PC Imaging

In theory, the single shot DW sequence and PC sequence are both sensitive to muscle motion in their magnitude image, and the PC sequence also allows quantification of velocity via its phase image. The implementation of the sequences differ in that the motion sensitization of the single shot DW sequence is described with a b -value while the PC sequence is described with a VENC. As such, both sequences can visualize motor unit activity and extract the contraction and relaxation time of muscle twitches (Fig. 4). The single shot DW sequence has the advantage that it is twice as fast; it only requires one acquisition per image, while the PC sequence requires two acquisitions per image. Each phase image is the difference image of two acquisitions: one with the velocity encoding gradients in one orientation and the second acquisition has the velocity encoding gradients in the opposite orientation. However, the single shot DW sequence only displays motion in arbitrary units of signal intensity on the magnitude

image, while the PC sequence allows quantification of bulk velocity using its phase image. Furthermore, the magnitude and phase image provide subtly different information about motor unit activity. Experimentally, the magnitude image is seen to detect only the active contraction and relaxation of the motor unit and provides sharper contrast detail between active and non-active muscle tissue. On the other hand, the phase signal detects both the active contraction and relaxation of a motor unit and any muscle fibers which are passively translated by the active muscle fibers. The DW signal is not influenced by this passive motion of muscle fibers as this motion is not incoherent. The boundaries of the active motor unit are therefore more difficult to observe on the phase image and the motor unit spatial extent will be overestimated. The magnitude image is therefore experimentally better for estimating the spatial extent of motor unit activity and the phase image better for assessing quantitative twitch profiles.

This raises the interesting question whether one can use the PC sequence to assess the magnitude image for the spatial extent of the motor unit and the phase image for the quantitative twitch profile. However, experimental work showed that for single motor units, the VENC should be 1–2 cm/sec, which equates to a b -value of $\sim 5 \text{ sec/mm}^2$. This b -value appears to be too low to generate enough contrast on the magnitude image of the PC sequence to detect the motor unit as a signal void. Higher b -values, i.e., 20 sec/mm^2 , lead to a VENC lower than 1 cm/sec, and induce aliasing in the phase signal.

Therefore, both sequences are needed to fully capture all information about muscle and motor unit activity. The single shot DW sequence is the preferred choice for imaging the spatial motor unit extent, either for imaging spontaneous muscle contractions or during controlled electrical stimulation. When interested in twitch dynamics under controlled electrical nerve stimulation, the PC sequence is the preferred choice.

Applications of Motor Unit MRI

Motor unit MRI has so far been used for three imaging applications 1) fasciculation, 2) motor unit area, and 3) motor unit twitch profile. Below, the goal of each application will be described, followed by an explanation of the data-acquisition (see also Table 1) and processing steps. Each section will end with an overview of the findings so far.

Fasciculation Imaging

The clinically most straightforward application of MUMRI is fasciculation imaging of muscles at rest. Fasciculation is the contraction of a group of skeletal muscle fibers due to spontaneous firing of a single lower motor neuron. Increased fasciculation rates are associated with early signs of lower motor neuron degeneration, making fasciculation an important

criteria in the diagnostic pathway of neuromuscular disorders, such as amyotrophic lateral sclerosis (ALS).^{24,25}

Data-Acquisition and Data-Processing

To observe fasciculation, resting muscle is imaged repetitively over several minutes with a single shot DW sequence (PGSE or PGSTE). The advantages of long versus short Δ (see section “Single shot DW sequences”) have not been fully explored in direct comparison. The acquired images are evaluated for short-lived signal voids, i.e., the spontaneously occurring fasciculation (Figs. 2 and 5a). For fasciculation imaging, higher b -values are recommended than for motor unit stimulation studies, because higher b -values increase the chance of detecting what are essentially random events. However, this is a trade-off with SNR, which will decrease with higher b -values due to true diffusion related signal attenuation making the fasciculation event undetectable from the image background noise. Experimental studies using b -values of 100–200 sec/mm^2 in healthy controls detected signal reductions in activated motor units to $\sim 20\%$ of baseline levels, again illustrating that this is not a diffusion phenomenon which requires much higher b values to obtain sensitivity. Surprisingly given that, muscle is a structured and orientated tissue; diffusion encoding direction seems to have little effect on the fasciculation detection sensitivity.^{14,15} This work is however, limited to small cohorts of healthy subjects. The effect of motion-sensitization times (δ and Δ) on the fasciculation detection sensitivity of PGSE and PGSTE sequences are part of ongoing studies. TE affects image contrast and noise level; TE should be as short as possible to maximize SNR, since skeletal muscle has a short T_2 relaxation time ($\sim 30 \text{ msec}$).²⁰ This can be achieved with parallel imaging, partial Fourier acquisition and PGSTE schemes. Per-slice TR is a trade-off between SNR, acquisition time and physiologically expected twitch duration. Shorter TR values reduce acquisition time, but induce T_1 weighting. Furthermore, TR should be at least 200 msec to avoid detecting the same fasciculation in two subsequent images (muscle twitch duration is ~ 200 – 300 msec).¹⁴ TR values of ~ 500 – 1000 msec have been used so far (Table 2).

Fasciculation analysis requires processing of the image time series to identify spatially contiguous groups of voxels (containing the underlying motor unit) which spontaneously fluctuate together from frame to frame. Preprocessing steps involve image registration and image denoising.²⁷ Thereafter, voxel-wise thresholding is applied testing for significant signal drops over time relative to a voxel's baseline signal producing fasciculation maps (Fig. 5b,c). Various algorithms have been used to detect fasciculation.^{14,15,28} Considerations include robustness for low and high fasciculation rates and exclusion of blood vessels, since they also show high temporal variation. Furthermore, partial volume effects should be addressed, eg, using a two-stage detection algorithm. This algorithm first

TABLE 1. Overview Sequence Settings Based on Currently Existing Literature for the Three MUMRI Applications

Sequence	Fasciculation imaging	Motor unit spatial extent	Motor unit twitch profile
	Muscle in rest	Muscle activated with electrical nerve stimulation	Muscle activated with electrical nerve stimulation
	PGSE or PGSTE	PGSE	PGSE or bi-polar PC
Settings	<ul style="list-style-type: none"> • $b \geq 100$: Trade-off with SNR, higher b-values are more sensitive, but have lower SNR • Minimal TE: To maximize SNR • $TR \geq 200$: To avoid detecting the same fasciculation twice • Fat suppression 	<ul style="list-style-type: none"> • $b \approx 10$–20 • Minimal TE: To maximize SNR • $TR \geq 500$: To ensure full relaxation of the muscle twitch between repetitive stimulations • Fat suppression 	<ul style="list-style-type: none"> • PGSE: $b \approx 10$–20 • PC • Full muscle twitch: 10–15 cm/sec • Single motor unit twitches: 1–2 cm/sec <p>To avoid aliasing, the VENC should exceed maximum expected velocity.</p> <ul style="list-style-type: none"> • Minimal TE: To maximize SNR • $TR \geq 500$: To ensure full relaxation of the muscle twitch between repetitive stimulations • Fat suppression

PC = phase contrast; PGSE = pulsed gradient spin echo; PGSTE = pulsed gradient stimulated echo; SNR = signal to noise ratio; TE = echo time; TR = repetition time.

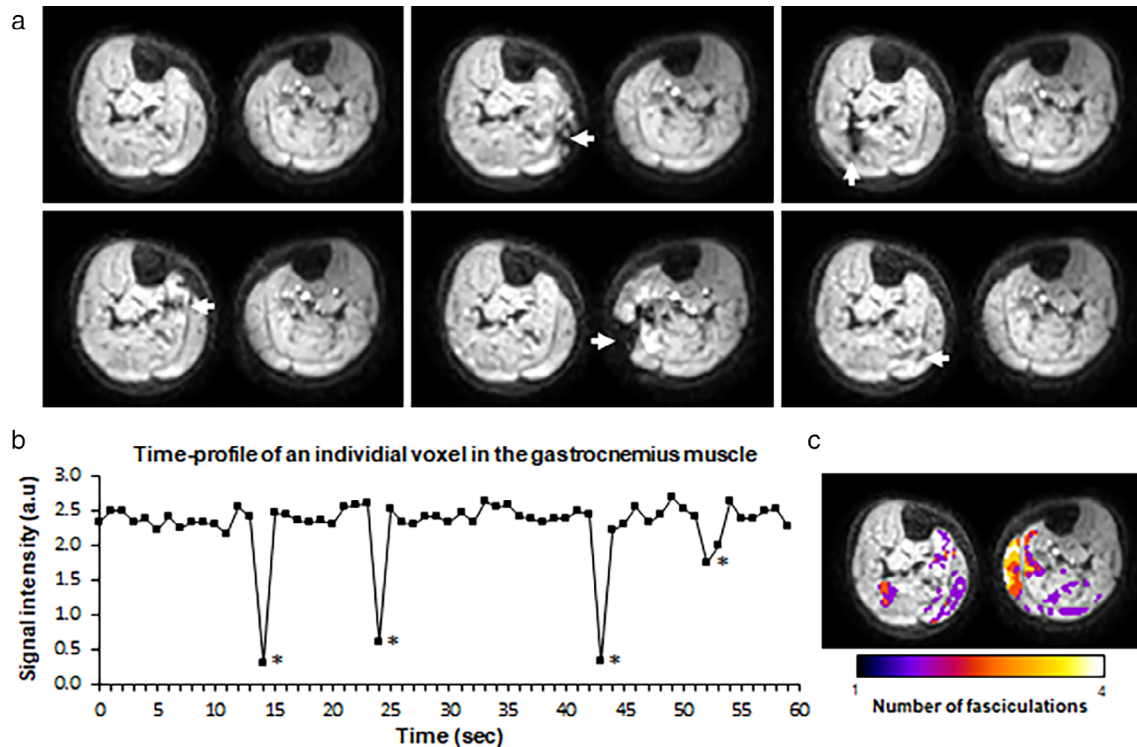


FIGURE 5: Fasciculation imaging with motor unit MRI. (a) Lower legs of a healthy volunteer imaged repetitively with a pulsed gradient spin echo (PGSE) sequence. Fasciculation (signal voids) are highlighted with white arrows in image 2–6 (image 1 shows no fasciculation). (b) Signal profile over 60 repetitive acquisitions of a single voxel in the gastrocnemius medialis showing four fasciculations, annotated with an asterisk. (c) Motor unit activity map displaying the number of fasciculation per voxel.

TABLE 2. Publication on Fasciculation Imaging in Humans in Chronological Order

Authors	Study population (n)	Body region(s)	MR sequence	Sequence settings	Fasciculation detection chance (%) [*]	Fasciculation detection rate (min ⁻¹) [*]
Steidle et al. ⁹	Healthy (n = 10)	Lower leg	PGSTE	$\Delta = 154$ msec $b = 100$ sec/mm ² 1000 images TR = 500 msec	20 ± 18	23.5 ± 21.7
Schwartz et al. ²³	Healthy (n = 3)	Lower leg	PGSE, SMS	$b = 100$ sec/mm ² 500 images TR = 500 msec	20 ± 10	23.0 ± 12.2
Schwartz et al. ¹⁸	Healthy (n = 8)	Lower leg	PGSTE	$\Delta = 157$ msec $b = 100$ sec/mm ² TM = 145 msec 960 images TR = 500 msec	16 ± 16	19.6 ± 19.2
Whittaker et al. ¹¹	ALS (n = 4) Healthy (n = 4)	Lower leg	PGSE	$b = 250$ sec/mm ² 1080 images TR = 1000 msec	ALS vs. healthy 27 (7–45) vs. 2 (1–3)	ALS vs. healthy 99.1 (25.7–161) vs. 7.7 (4.3–9.7)
Otto et al. ²⁶	SMA (n = 1) Healthy (n = 4)	Upper legs	PGSE	$B = 200/400/600$ sec/mm ² TR = 5000 msec	SMA vs. healthy 14 vs. 4 ± 3	SMA vs. healthy 21.0 vs. 5.2 ± 4.2
Schwartz et al. ²⁷	Suspected neuromuscular disease (n = 3) Healthy (n = 6)	Tongue Shoulder Lower legs	PGSTE	$\Delta = 148$ or 28 msec $b = 100$ sec/mm ² TR = 500 msec	Disease vs. healthy Tongue: 49 ± 46 vs. 8 ± 9 Shoulder: 85 ± 21 vs. 13 ± 3 Lower legs: 47 ± 47 vs. 25 ± 42	N/A
Heskamp et al. ²⁵	ALS (n = 10) Healthy (n = 10)	Tongue Biceps brachii Paraspinals Lower legs	PGSE	Tongue: $b = 20$ sec/mm ² Other regions: $b = 200$ sec/mm ² 240 images/region TR = 1050–1125 msec	ALS vs. healthy Tongue: 27 ± 35 vs. 6 ± 6 Biceps brachii: 13 ± 12 vs. 1 ± 3 Paraspinals: ± 113 vs. 2 ± 2 Lower legs: 167 ± 174 vs. 20 ± 18	ALS vs. healthy Tongue: 1.0 ± 1.3 vs. 0.2 ± 0.2 Biceps brachii: 0.5 ± 0.4 vs. 0.0 ± 0.1 Paraspinals: 2.0 ± 4.0 vs. 0.1 ± 0.1 Lower legs: 6.3 ± 6.6 vs. 0.7 ± 0.7

^{*}Fasciculation detection chance is the number of detected fasciculation divided by the number of analyzed images x 100%, and the fasciculation detection rate is the number of fasciculations divided by the acquisition time in minutes. Numbers are estimated based on the published data. N/A: values cannot be estimated from the published data. ALS = amyotrophic lateral sclerosis; PGSTE = pulsed gradient stimulated echo; PGSE = pulsed gradient spin echo; SMS = simultaneous multi slice; TR = repetition time; SMA = spinal muscular atrophy.

detects areas with significant signal drop and uses those regions as seeding-points for graph-based segmentation to include neighboring voxels with the same time-profile.²⁵ Furthermore, deep-learning methods to detect fasciculation are under development.²⁹

Fasciculation can be quantified as the number of events detected within a time series of images. However, for comparison between studies data requires scaling to scan duration and sampling volume.

Findings

In vivo MUMRI fasciculation imaging has been described in several publications, but as a relatively young field there is also

important data in conference abstracts. The study populations, sequence settings and estimated fasciculation detection chance and fasciculation rate are summarized in Table 2.

The first spatial distribution images of fasciculation were obtained in healthy people. In this study,¹⁴ the lower legs of 10 healthy subjects were imaged, with all subjects displaying fasciculation on the acquired images. The fasciculation rate varied widely between participants and muscles and was on average $23.5 \pm 21.7 \text{ min}^{-1}$. The highest fasciculation rates were observed in the soleus and gastrocnemius (Fig. 6a), independent of diffusion encoding direction. The fasciculation size was 1.5 to 2.5 cm in the transverse plane and 1.5 to 7 cm in the proximo-distal direction (Fig. 6b). Lower leg fasciculations have been

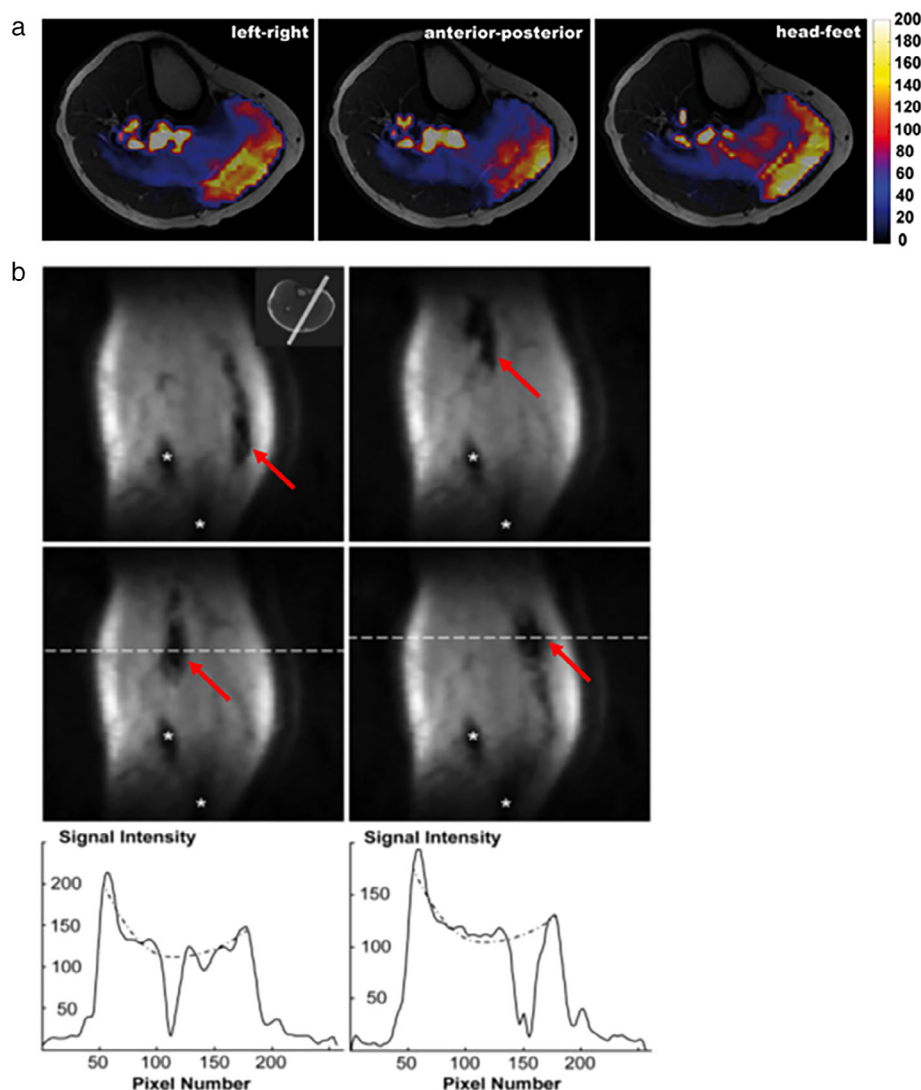


FIGURE 6: The first published fasciculation maps in the lower legs of healthy subjects and four typical examples of fasciculation in the proximo-distal direction. (a) Fasciculation maps were created for three diffusion encoding direction. The color bar indicates the number of detected fasciculations per voxel over 1000 consecutive images. All three directions show similar fasciculation maps with the highest number of fasciculations observed in the gastrocnemius medialis and soleus. Data were recorded in a 33-year old healthy male subject. (b) Images were acquired with oblique slice orientation. Areas with low signal intensities belonging to bone are indicated by the white asterisks, the other areas with low signal intensities are the fasciculation (indicated by the red arrows). For the bottom row, the signal profile is displayed for the dashed white line, revealing a signal reduction to almost the noise level during a fasciculation. Receiver-characteristics of the eight-channel knee coil are indicated by dotted lines in the signal intensity graphs. Figures re-used and combined with permission from Steidle et al.¹⁴

assessed in 3D by acquiring four slices simultaneously and combined this with diffusion tensor imaging (DTI) fiber tracking.²⁵ The cross-sectional area (CSA) of the fasciculations ranged from ~ 10 to 800 mm^2 ; fasciculations in the soleus had the largest CSAs (median: $\sim 150 \text{ mm}^2$). A fasciculation CSA made up 0.18% to 10% of the individual muscle CSA. The majority of the fasciculations were visible on adjacent slices. This means that the proximo-distal length of a fasciculation ranges from 1.8 cm to at least 5.4 cm. According to the DTI fiber tracks, the signal voids that presented at subsequent slices were connected by muscle fibers. However, only four slices were examined; thus, definite conclusions on motor unit size along the length of the muscle require further investigation.

MUMRI fasciculation imaging can be combined with in-scanner sEMG recordings, but gradient switching during the MRI acquisition distorts the EMG trace with 300-fold higher amplitude compared to electrical activity induced by fasciculation. These gradient-induced distortions can be removed using template based subtraction,¹⁹ which enables detection of small fasciculations potentials in the sEMG trace (Fig. 7). Using this approach, the lower leg of eight healthy people were imaged and the electrical activity in the gastrocnemius medialis was recorded simultaneously. The number of MUMRI-detected fasciculations correlated with the number of sEMG-detected fasciculations, but the average fasciculation rate was higher with MUMRI compared to sEMG ($\sim 19 \text{ min}^{-1}$ vs. $\sim 9 \text{ min}^{-1}$). Within 15 mm around the sEMG electrodes, $91.3\% \pm 10.9\%$ of the MUMRI-detected fasciculations were related to sEMG-detected fasciculations. This dropped to $36.1\% \pm 16.7\%$ when this region was increased to 30 mm. Furthermore, 60.4% of all sEMG-

detected fasciculations were mapped to a MUMRI-detected fasciculation. The other 39.6% could not be mapped, most likely because the muscle contraction took place outside the motion sensitive phase of the PGSTE sequence (Fig. 7). From this, they concluded that sEMG activity that takes place up to 300–350 msec till the end of MRI sequence's motion-sensitive period ($\Delta = 157 \text{ msec}$), will be visible on PGSTE images. Recently, a neural network was developed to remove gradient-induced artefact in the EMG, which outperformed the template subtraction method.²⁶

Spontaneous myoelectric activity measured with in-scanner EMG trace can also be used to trigger the MUMRI acquisition to be time-locked to muscle twitch associated with the EMG activity. Proof of principle measurement in two healthy volunteers showed fasciculation on all EMG-triggered MUMRI images, and none of the non-triggered MUMRI images.²¹ This set-up has two main advantages. First, fasciculations can be systematically examined with MUMRI at different points in the contraction and relaxation cycle. Of note, fasciculation is a random process; therefore, it is unlikely that the exact same fasciculation will be imaged repetitively. Second, the EMG trace can be retrospectively examined to discriminate true fasciculation and volitional activity, something difficult to differentiate on MUMRI alone.³⁰

The most obvious diseases that could benefit from fasciculation imaging are motor neuron diseases, like ALS and SMA, as one of the presenting symptoms is fasciculation. The first patient study was indeed performed in ALS and confirmed that MUMRI is capable of detecting the increased fasciculation rate expected in ALS patients compared to healthy controls (ALS: 99.1 min^{-1} vs. healthy: 7.7 min^{-1})¹⁶ (Fig. 8). The fasciculations CSA covered a larger portion of the muscle in ALS patients ($15.9\% \pm 2.8\%$) compared to healthy controls ($2.9\% \pm 1.6\%$). This was followed by a case-report study in a presymptomatic SMA patient, who showed significantly more fasciculations in the upper legs compared to four healthy controls (45.5 vs. 13.5 ± 10.9).³¹ These findings gave a first hint that MUMRI can detect early signs of lower motor neuron degeneration.

The earliest MUMRI studies in both healthy and disease were limited to the lower extremity only, while ALS is especially known for its heterogeneous disease onset. Therefore, diagnosing ALS solely on lower motor neuron dysfunction, eg, on fasciculation, requires presence of fasciculation in at least two body regions.²⁴ Body regions are defined based on their innervation level, i.e., bulbar, cervical, thoracic, and lumbosacral. Therefore, the first steps were taken to extend MUMRI fasciculation imaging toward multiple body regions, including the tongue, upper arm, shoulder, paraspinal, and bilateral upper and lower leg muscles.^{28,29} Body regions were initially scanned based on clinical symptoms.²⁹ They found a higher fasciculation detection chance in four patients with suspected neuromuscular disorder compared to six healthy controls for

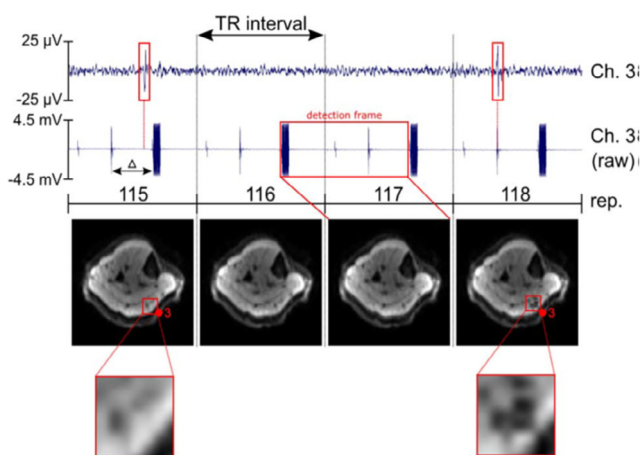


FIGURE 7: The sEMG recordings in the gastrocnemius medialis during motor unit MRI (MUMRI) with a PGSTE sequence. The artefact-corrected sEMG signal (top) shows two spontaneous sEMG activities (red rectangles). The raw sEMG signal is displayed at the bottom, and clearly shows the artefacts induced by the MR gradient switching. The red box indicates the detection period for one MUMRI acquisition. Two sEMG activities are perceptible, but only the second one is visible on MUMRI. Figure re-used with permission from Schwartz et al.²¹

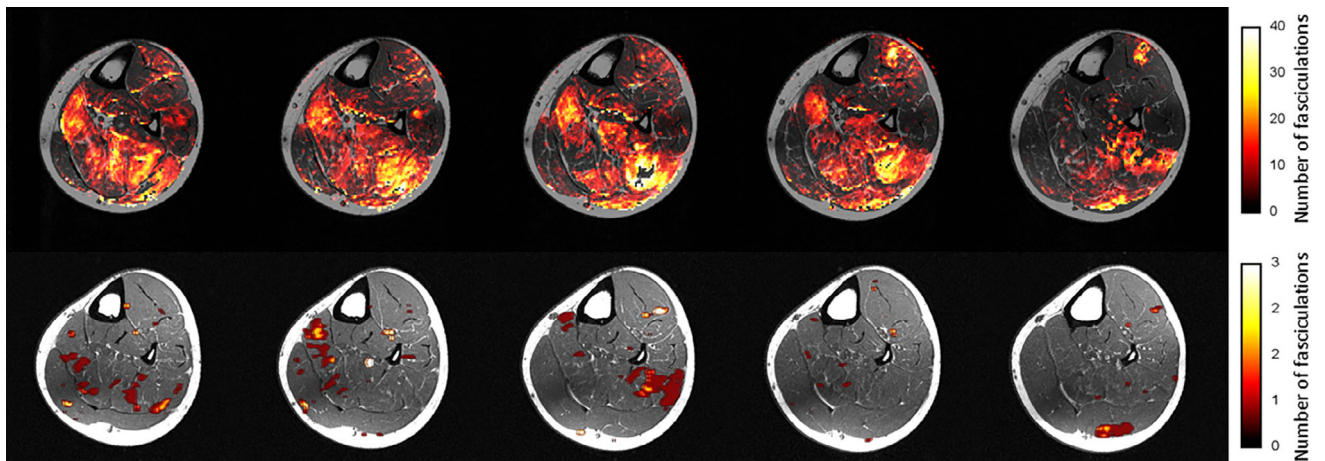


FIGURE 8: Example of fasciculation maps in an ALS patient compared to a healthy control. Top row—number of fasciculation in a patient with ALS from five slices of pulsed gradient spin echo data, overlaid onto structural T1 weighted images, color scale runs from 0 to 40 events. Bottom row—number of fasciculation in a healthy control. Note, the scale here runs from 0 to 3 events, due to the control having so few fasciculation. Unpublished data from our group.

the lower leg ($47\% \pm 47\%$ vs. $25\% \pm 42\%$), shoulder ($85\% \pm 21\%$ vs. 13 ± 3), and tongue ($49\% \pm 46\%$ vs. $8\% \pm 9\%$). They also made the interesting observation that in patients with high fasciculation rates, the PGSTE sequence with $\Delta = 145$ msec is too sensitive to motion, and used $\Delta = 28$ msec instead. A similar whole body approach was developed in a subsequent study,²⁸ which systematically examined the tongue, biceps brachii, paraspinals, and lower leg muscles in 10 ALS patients and 10 healthy controls. Median fasciculation rates in ALS patients were significantly higher compared to healthy controls for biceps brachii ($0.5 \pm 0.4 \text{ min}^{-1}$ vs. $0.0 \pm 0.1 \text{ min}^{-1}$), paraspinals ($2.0 \pm 4.0 \text{ min}^{-1}$ vs. $0.1 \pm 0.1 \text{ min}^{-1}$) and lower legs ($6.3 \pm 6.6 \text{ min}^{-1}$ vs. $0.7 \pm 0.7 \text{ min}^{-1}$), but not the tongue ($1.0 \pm 1.3 \text{ min}^{-1}$ vs. $0.2 \pm 0.2 \text{ min}^{-1}$). Furthermore, 9/10 ALS patients showed increased levels of fasciculation compared to healthy controls in at least one of their body regions (Video A).

Imaging of the Motor Unit Area

Instead of waiting for random spontaneous motor unit firing, MUMRI can also be combined with in-scanner electrical nerve stimulation to activate motor units.¹⁶ This enables controlled imaging of motor unit areas. The feasibility of this approach was presented for the first time by Whittaker et al.¹⁶ and fine-tuned for single motor unit imaging by Birkbeck et al.³²

Data-Acquisition and Data-Processing

With MUMRI electrical stimulation studies, the muscle of interest is repetitively imaged with a PGSE sequence while electrically stimulating the muscle's innervating nerve, employing standard neurophysiological paradigms. The imaging sequence's motion-sensitive window is synchronized with the muscle's maximum contraction rate during the twitch to achieve maximum contrast. Activated motor

units then appear dark on the image relative to surrounding non-activated muscle tissue (Fig. 9). Unlike fasciculation imaging, b -value of $10\text{--}20 \text{ sec/mm}^2$ are recommended as there is progressive activation of motor units until the muscle is fully active (Video B).^{16,32} At $b = 200 \text{ sec/mm}^2$ the signal very quickly saturates. Furthermore, to ensure full muscle relaxation in-between two subsequent stimuli, the interstimulus interval should be longer than the twitch duration (up to ~ 300 msec), eg, stimulation frequencies of maximally $\sim 2 \text{ Hz}$. This stimulation frequency then determined the interslice excitation, i.e., 500 msec for 2 Hz stimulation.

For single motor unit imaging, low current stimulation is required to activate a limited number of individual motor units. The required current level is determined experimentally by gradually reducing the stimulation current in very small steps (order of 0.01 mA) until no motor unit activity remains. The small steps in current are required to observe motor unit alternation, i.e., when a motor unit is stimulated near its firing threshold, it will sometimes fire and sometimes not. Consequently, the motor unit alternately discharges in some images, while it does not discharge in other images (Fig. 9b,c) (Video C). Motor unit alternation is considered a definitive demonstration that the signal change in the involved region of voxels observed represents the structure of a single motor unit. In published work, motor unit alternation has been used to create motor unit activity maps and extract single motor unit extent (Fig. 9b–d).^{32,33} The spatial extent of a motor unit can be presented as the CSA and maximum and minimum Feret diameter (Fig. 10a). Other data-analysis approaches such as correlation metrics (i.e., correlating active pixels based on their temporal evolution across the time series) are worth exploring to speed up the analysis time.

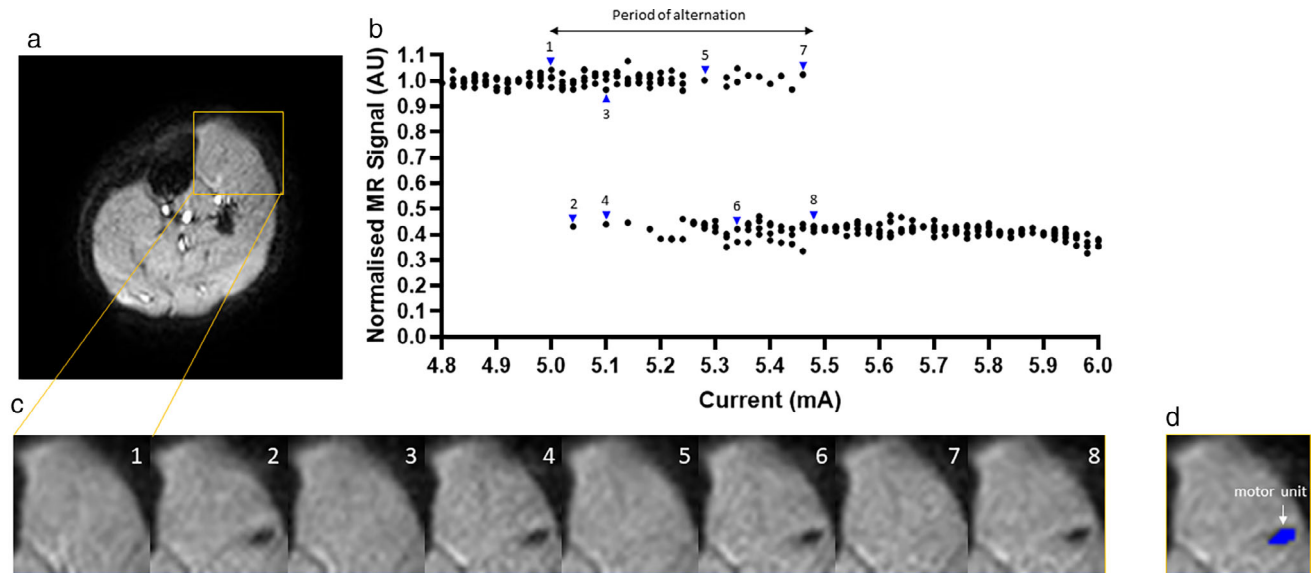


FIGURE 9: Motor unit territory imaging with motor unit MRI. (a) Pulsed gradient spin echo (PGSE) image of the lower leg. The orange rectangle represents a subset of the image shown as close-up in (c,d). (b) The signal intensity of a single voxel displayed against the stimulation current in a motor unit in the tibialis anterior. This single motor unit begins alternating at 5 mA (arrow 1) and stops alternating and becomes continuously active at 5.48 mA (arrow 8). (c) Close-ups of the tibialis anterior muscle of the PGSE image from A. The motor unit is visible at time-point 2, 4, 6, and 8, and not visible at time-point 1, 3, 5, and 7. The motor unit is depicted by the blue arrowheads. (d) The extracted motor unit territory of the single motor unit (in blue) overlaid on a close-up of the PGSE image from (a).

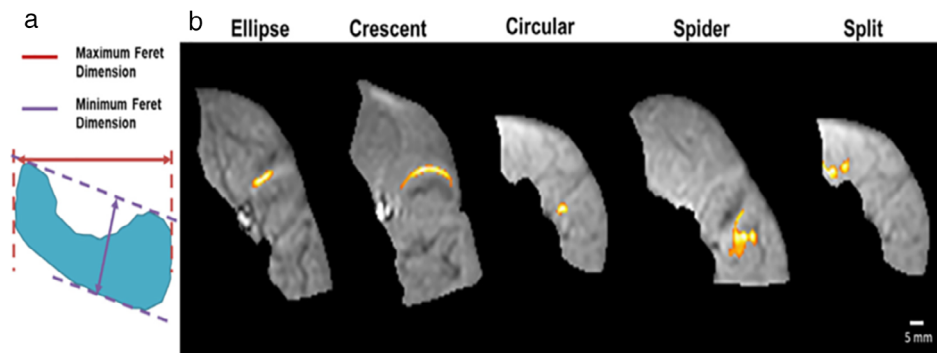


FIGURE 10: Classification of motor unit size and shape. (a) Schematic representation of the maximum (red arrow) and minimum Feret diameter (purple arrow). (b) Typical examples of the five detected motor unit shapes. All examples are following peroneal nerve stimulation and occur within the muscles of the anterior compartment of the leg. This anterior compartment has been segmented out from the full lower leg. Figure re-used with permission from Birkbeck et al.³²

Findings

In 2020, the first ever systematic *in vivo* images of the 2D spatial extent of individual motor units were published.³² Thirty-one individual motor units were measured in the lower leg during peroneal nerve or tibial nerve stimulation; per subject a median of three motor units were detected for peroneal nerve stimulation and one motor unit for tibial nerve stimulation. Most motor units were observed in the peroneus longus and extensor digitorum. Motor units were classified according to their shape: elliptical, crescent, circular, spider, and split. The most common shape was elliptical (19/31 motor units), followed by crescent (5/31) (Fig. 10b). These shapes are consistent with *ex vivo* glycogen depletion

experiments, in which a single motor unit is stimulated until the glycogen stores in the muscle fibers this axon innervates are selectively depleted. These fibers can then be mapped as an innervated territory.^{2,34} Two motor units were split into two separate regions with highly correlated time-series. The intervening area of muscle, which showed no activity, is consistent with the electrically silent regions sometimes seen with scanning EMG.³⁵ Whether these seemingly discrete regions coalesce to form a contiguous structure further along the muscle could not be determined as only a single slice was acquired. The average motor unit CSA was $26.7 \pm 11.2 \text{ mm}^2$ and the maximum and minimum Feret diameter were $10.7 \pm 3.3 \text{ mm}$ and $4.5 \pm 1.2 \text{ mm}$, respectively.

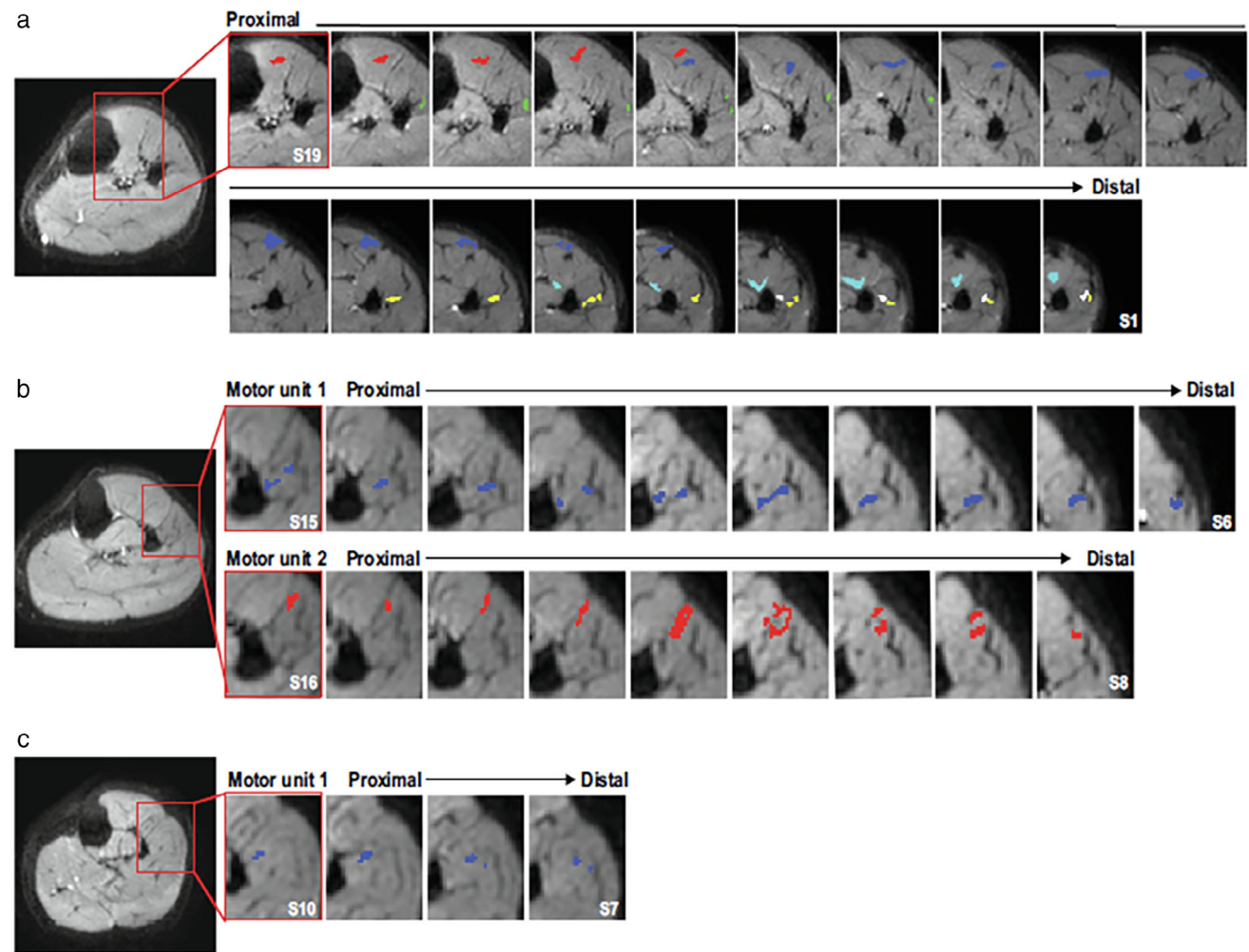


FIGURE 11: Typical examples of 3D motor unit maps along the motor unit length for three participants. (a) Distribution of six motor units detected by alternation behavior under nerve stimulation in one participant along the lower leg from the most proximal slice (top left, slice 19) to the most distal slice (bottom right, slice 1). Each motor unit is depicted in a different color. The motor units in dark blue, light blue and yellow show a significant change in size and shape along the motor unit length, being largest in the middle part of the motor unit. Interestingly, the green and yellow motor unit split in two or three distinct areas in the middle part of the motor unit, while being one area at the distal and proximal ends. The red and white motor unit show only minimal variation in size and shape along the motor unit length. (b) Motor unit maps of another participant displaying two motor units from the most proximal slice that the motor unit was visible (left) to the most distal slice (right), again exhibiting the largest motor dimensions in the middle part of the motor unit. Motor unit 2, colored red, first appears in slice 8 as a single territory, splits into two spatially distinct territories in slice 9 and 10, before re-coalescing into a single territory at slice 11. (c) Motor unit maps of a third participant displaying a 4 cm long motor unit split into two units. Figure re-used with permission from Heskamp et al.³³

The technique was subsequently applied to other body regions and optimized toward shorter acquisition times by increasing the stimulation step size from 0.01 mA to 0.03 m.³³ This brought the acquisition time down from 18 to 6 minutes. A total of 27 motor units were imaged in the lower legs anterior compartment, 19 motor units in the forearms flexor carpi ulnaris and flexor digitorum profundus and 16 motor units in hands abductor pollicis brevis and opponens pollicis. The most common motor unit shape was again elliptical. The average motor unit CSA did not differ between body regions (lower legs: $22.4 \pm 8.4 \text{ mm}^2$, forearm: $23.6 \pm 14.1 \text{ mm}^2$, hand: $26.8 \pm 12.8 \text{ mm}^2$). This implies that the area occupied by a single motor unit relative to the activated muscle CSA

was larger in the hand compared to the legs and forearm. This in turn suggests that hand muscles contain fewer motor units or hand motor units have more overlap. The former is in line with literature.^{3,36–38}

Motor units extend along the length of the muscle they constitute³⁹; therefore, a 3D approach to study single motor units was developed and 15 motor units in the lower legs were examined in 3D using a multislice acquisition.³³ Average motor unit length was $8.0 \pm 3.8 \text{ cm}$ (range 4.0–19.0 cm); none of the motor units extended all the way from the distal tendon to the proximal tendon. Motor unit CSA and shape varied along the motor unit's proximo-distal axis (Fig. 11). The CSA was largest in the middle of the motor unit and smallest at proximo-distal edges. The motor unit shape also

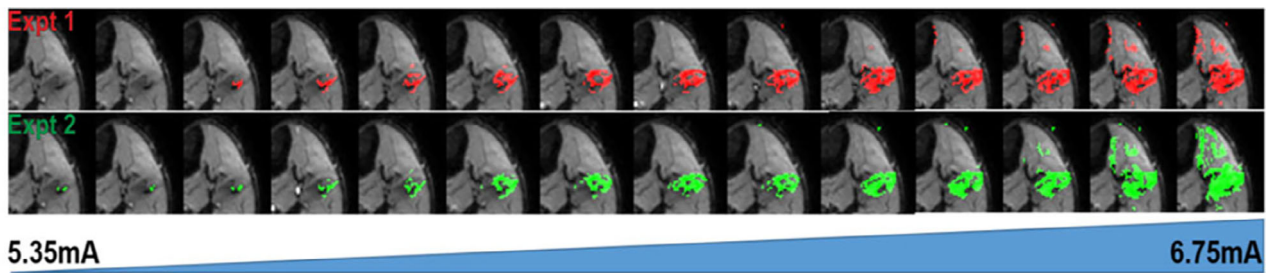


FIGURE 12: Recruitment of discrete regions of motor unit activity within the lower leg's anterior compartment. (a) The lower leg imaged during gradually increased in-scanner electrical nerve stimulation of the peroneal nerve, the colored pixels display the recruited regions, i.e., voxels displaying significant signal drop at this given time-point. The area of the recruited voxels gradually increases with increasing stimulation current. An almost identical recruitment pattern is observed for run 1 (top row, in red), and run 2 (bottom row, green), acquired 5 minutes later. Figure re-used with permission from Whittaker et al.¹⁶

changed along the proximo-distal axis, 8 out of 15 motor units split into 2 or 3 subunits at some slices and coalesced again into a single unit at other slices. The maximum CSA over the whole motor unit was twice as large as the CSA assessed only at a single slice. This has major implications for quantitative studies using single-slice MUMRI or scanning EMG, as single cross-sections may not accurately reflect the whole motor unit size. Consequently, the same cross-section should be examined every time to minimize measurement variations.

The studies discussed above imaged single motor units. Potentially, MUMRI can examine the recruitment order of a larger portion of the motor unit pool and estimate the number of motor units in the stimulated muscle and the average motor unit size, as an equivalent to neurophysiology motor unit estimation techniques.⁴⁰ Proof of this principle was shown by increasing the stimulation current in coarse steps (0.05 mA) and quantifying the recruitment of discrete regions, which was repeatable over subsequent runs¹⁶ (Fig. 12).

Imaging of Motor Unit Twitch Profile

MUMRI combined with repetitive electrical nerve stimulation can also be used to measure twitch profiles of skeletal muscles and individual motor units.^{16,22} As discussed in section “[Technical background to Motor unit MRI](#),” a PGSE or PC sequence can be used. In both situations, the stimulation current is fixed and for each repetitive acquisition, the timing between the electrical stimuli and imaging acquisition window is shifted such that the motion sensitive period is moved step-wise along the muscle twitch profile (Fig. 4).

Data-Acquisition and Data-Processing

For the PGSE sequence, settings are optimized as discussed in section “[Imaging of the motor unit territory](#).” For the PC sequence, the VENC needs to be carefully chosen to avoid signal aliasing; 10–15 cm/sec has been used for full muscle twitches and 1–2 cm/sec for single motor unit twitches. For single motor unit imaging, the stimulation current should

continuously activate a single motor unit without alternation.²² The electrical stimulus pulse timing needs to be varied relative to the motion sensitive period in order to capture the full muscle twitch profile; published studies used a sequence TR of 1 sec and altered the timing of the stimulation pulse from ~45 msec after the 90° RF pulse to ~400 msec before the 90° RF pulse (step size: 5 msec) (Video D).

To extract the PGSE twitch profile or PC velocity profile, the average signal intensity (or velocity) is determined at each time-point over the area of interest, eg, whole muscle or individual motor unit. The integral of the PC velocity profile gives the PC displacement profile. More post-processing details can be found in Heskamp et al.²²

The PGSE twitch profile and PC velocity and displacement profiles can be used to quantify motor unit dynamics by calculating, eg, the contraction and relaxation time (Fig. 4c,d). In addition, the maximum contraction velocity, maximum relaxation velocity, and maximum displacement can be calculated from the PC velocity and displacement profile.

Findings

The twitch profile of the lower leg's full anterior compartment has been measured with a PGSE sequence.²² The average MRI measured contraction time was 103 ± 20 msec and correlated with contraction time measured with a force rig (this was a custom-built MR compatible device that can be used to measure the force output from electrical nerve stimulation. The participants' foot was strapped into the foot holder and force output measured using a load cell attached to the back of the foot holder). Application of this technique to single motor units revealed a clear signal attenuation during motor unit contraction, but signal attenuation during motor unit relaxation is more variable in magnitude (Fig. 13). In contrast, velocity profiles obtained during PC measurements of these motor units did show the relaxation phase as a negative velocity lobe. The absence of the relaxation phase in the PGSE obtained signal profile of single motor unit twitches is as yet unexplained. The contraction and relaxation velocity of single motor units was on average

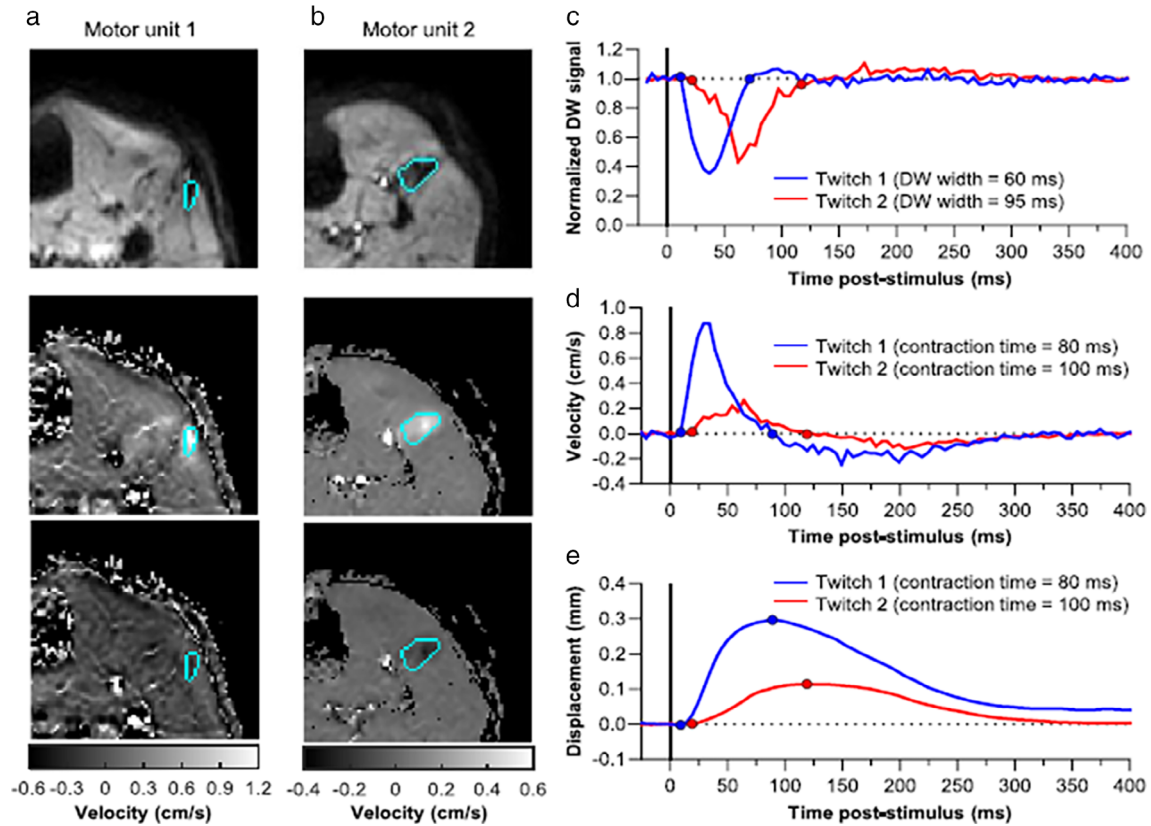


FIGURE 13: Typical examples of pulsed gradient spin echo (PGSE) and PC images during the contraction or relaxation phase of single motor units. (a,b) Two typical examples of a motor unit (delineated in light blue) on a PGSE image (top) and PC image (middle/bottom). The PGSE image is shown at the time point that the PGSE signal reaches its maximum signal drop. The PC images are shown for the time point with maximum velocity (middle) and minimum velocity (bottom). (c) Normalized PGSE signal intensity displayed against the time post stimulus for the motor units shown in (a,b, and d) Velocity profile measured with the PC sequence. (e) Displacement profile (integrated velocity signal). The start and end of the contraction period are depicted in circles. Figure re-used with permission from Heskamp et al.²²

0.55 ± 0.26 cm/sec and 0.22 ± 0.11 cm/sec, respectively. This equaled an average muscle fiber displacement of 0.20 ± 0.10 mm. Single motor unit contraction times assessed with PGSE (75 ± 13 msec) and PC (81 ± 15 msec) were highly correlated, but there is a significant offset between the two techniques. This offset is caused by the convolution between the true twitch profile and the response of the imaging acquisition window, which depends on the Δ of the sequence. This offset is estimated via simulations (linear correlation between contraction time of the input twitch and modeled MRI signal for several contraction times). Subtracting this offset from the MRI measured contraction time, gives the actual contraction time.²² This results in single motor unit contraction times in line with literature.^{4,34,41,42} The PC sequence has also been used to image whole muscle and single motor unit twitch profiles in a large cohort of healthy adults (aged 26–82 yr).⁴³ Both age and sex positively predicted an increased whole anterior compartment contraction and relaxation time, with older females showing the longest contraction and relaxation times. This suggests that PC twitch imaging can detect physiological

changes related to age that occur within muscle. Second, measured contraction and relaxation times of single motor units demonstrated no change with participant age, which may be explained by the non-physiological and potentially random pattern of motor unit recruitment observed when using electrical nerve stimulation.⁴⁴

Outlook

Clinical Potential

Patients with motor neuron diseases face significant diagnostic delays, because current diagnostic techniques can lack sensitivity to the earliest signs of motor neuron loss. Furthermore, clinical trials of novel therapies are hampered by a lack of objective biomarkers. MUMRI shows promise in both these areas. Fasciculation is an early sign in ALS, and provides evidence of early motor neuronal loss. Whole-body fasciculation imaging could be of clinically significant for motor neuron diseases, by providing non-invasive assessments of disease spread through the body and improving diagnostic sensitivity by guiding needle EMG or ultrasound assessments. MUMRI also shows

potential in detecting and quantifying later changes in motor unit structure resulting from re-innervation.

MUMRI fasciculation imaging extends to other neuromuscular disorders such as SMA and has applications in studies of ageing and exercise. Preliminary findings, presented in conference proceedings, suggest an age-related increase in fasciculation rate.⁴⁵ Furthermore, imaging re-innervation and muscle twitch profiles with MUMRI can visualize motor unit recruitment patterns and fiber type distribution or conversion. This can give insight into the partly unexplained muscle weakness in ageing vs. sarcopenia and will benefit exercise physiology studies. Furthermore, detecting motor unit recruitment patterns or changes in muscle twitch profiles could contribute to understanding aspects of fatigue in neuromuscular disorders, like chronic inflammatory demyelinating polyneuropathy.⁴⁶

Limitations of MUMRI Compared to Other Techniques and Future Improvements

MUMRI offers unique capabilities by simultaneously imaging multiple muscles at once, both deep and superficial muscles, and providing 2D or 3D spatial information on motor unit size, shape and position. This cannot be achieved with two other widely applicable techniques: EMG and ultrasound. EMG measures only the electrical signal, lacking spatial information. Ultrasound has a much higher temporal resolution compared to MUMRI, but has a small field of view, limited to superficial muscles, and does not show clear motor unit edges. MUMRI reaches a typical 1.5 mm in-plane resolution, constrained by the EPI readout, and 5–10 mm through-plane. Consequently, the motor unit edges are coarsely displayed and sometimes difficult to distinguish. Also, for 3D assessments in electrical stimulation studies, stimulation steps are performed per slice, lengthening the acquisition. This could be overcome by using simultaneous multislice imaging.⁴⁷

While theoretically applicable to all skeletal muscles, practical challenges exist, especially in regions like the upper limbs. The arms are generally positioned close to the edge of the scanner bore, where B_0 homogeneity is poorest. In patients with low to normal body habitus, the image quality can be optimized by moving the limb-side of interest closer to the magnet iso-center; however, this is not possible for all patients. This issue does not exist with ultrasound and neurophysiology techniques. Furthermore, MUMRI cannot yet image the diaphragm, while ultrasound can.

The temporal resolution of MUMRI (0.5–1 sec) is much lower than EMG and ultrasound (order of msec or μ sec), posing challenges for twitch profile imaging. Workarounds are possible with repetitive stimulation and overall long acquisition times.²² Further developments will likely improve the temporal resolution of MUMRI, but it will never match ultrasound and EMG.

Specific for the electrical stimulation studies, MUMRI faces limitations in detecting multiple motor units due to significant signal attenuation from a single motor unit contraction. Consequently, in experiments performed so far motor unit size and twitch profile measures have been limited to one or a few motor units per subject.^{32,33} Estimates of the total number of motor units and their average size is therefore not possible yet, but development is ongoing to optimize scanning methodology.

In general, MRI scanning is more costly and more burdensome compared to ultrasound and EMG. However, most if not all patients under investigation for neuromuscular disorders in which MUMRI may be useful—such as motor neuron disease—currently undergo MRI as part of their diagnostic work-up. Adding MUMRI to an existing MRI examination would be significantly cheaper and less involving.

Implementation in clinical practice varies depending on the application. MUMRI fasciculation imaging is straightforward and can be incorporated in clinical protocols, utilizing a standard PGSE sequence available on every modern clinical MRI scanner. Motor unit territory and twitch profile imaging are currently limited to specialized centers and are less likely to transfer to clinical protocols, because they require complex in-scanner electrical stimulation hardware and software. Ongoing research aims to explore alternative methods for controlled motor unit activation without electrical stimulation, eg, via volitional exercise protocols.

Finally, optimal application of MUMRI necessitates a deeper understanding of its contrast mechanism, as some observations remain unexplained. For example, simulations have clearly demonstrated that the major signal voids are due to intravoxel contraction; however, in experimental data these signal voids are often accompanied by hyperintense areas around or near the signal voids. Furthermore, the relaxation phase in single motor unit twitch measurements with PGSE often does not show a signal attenuation and sometimes instead even a slight signal increase. In theory, hyperintensities on MUMRI images could be due to increased T_2 relaxation time (T_2 shine-through), decreased tissue movement or increased proton density. However, from a physiological point-of-view, none of these factors can be large enough to account for the observed signal hyperintensity.²² Another potential explanation is T_1 saturation, due to new tissue water moving into the slice that were not excited in the previous TR, but this requires further investigation.

Conclusion

This review has introduced the current state of the art in the new MRI application of motor unit imaging, called “motor unit MRI or MUMRI”. The experimental data clearly show the ability of single shot DW sequences and PC sequences to identify motor units, to measure spontaneous activity and to

quantify morphology or twitch profiles when the method is combined with electrical nerve stimulation. Clinical application of MUMRI is at present limited to small scale studies. However, even with small group sizes the ability to differentiate between patients with ALS and healthy volunteers appears to have high sensitivity,^{16,29} setting the scene for MUMRI as an important diagnostic advancement for neuromuscular diseases. To demonstrate this clinical potential requires larger scale adoption and use in prospective trials.

References

1. U. C. London. About neuromuscular diseases|Queen Square Centre for Neuromuscular Diseases. <https://www.ucl.ac.uk/centre-for-neuromuscular-diseases/about-neuromuscular-diseases>.
2. Edström L, Kugelberg E. Histochemical composition, distribution of fibres and fatiguability of single motor units. Anterior tibial muscle of the rat. *J Neurol Neurosurg Psychiatry* 1968;31(5):424-433.
3. Duchateau J, Enoka RM. Distribution of motor unit properties across human muscles. *J Appl Physiol* 2022;132(1):1-13.
4. Andreassen S, Arendt-Nielsen L. Muscle fibre conduction velocity in motor units of the human anterior tibial muscle: A new size principle parameter. *J Physiol* 1987;391:561-571.
5. Enoka RM, Farina D. Force steadiness: From motor units to voluntary actions. *Phys Ther* 2021;36(2):114-130.
6. Brannagan TH, Hays AP, Lange DJ, Trojaborg W. The role of quantitative electromyography in inclusion body myositis. *J Neurol Neurosurg Psychiatry* 1997;63:776-779.
7. Lunn MR, Wang CH. Spinal muscular atrophy. *Lancet (London, England)* 2008;371:2120-2133.
8. Mallik A. Nerve conduction studies: Essentials and pitfalls in practice. *J Neurol Neurosurg Psychiatry* 2005;76:ii23-ii31.
9. Carlier PG, Azzabou N, de Sousa PL, et al. Skeletal muscle quantitative nuclear magnetic resonance imaging follow-up of adult Pompe patients. *J Inher Metab Dis* 2015;38(3):565-572.
10. Strijkers GJ, Araujo ECA, Azzabou N, et al. Exploration of new contrasts, targets, and MR imaging and spectroscopy techniques for neuromuscular disease—a workshop report of working group 3 of the biomedicine and molecular biosciences COST action BM1304 MYO-MRI. *J Neuromuscul Dis* 2019;6(1):1-30.
11. Kriss A, Jenkins T. Muscle MRI in motor neuron diseases: A systematic review. *Amyotroph Lateral Scler Front Degener* 2022;23(3-4):161-175.
12. Kaufmann L, Gruber B, Gerstman D, Kaell A. Preliminary observations on the role of magnetic resonance imaging for polymyositis and dermatomyositis. *Ann Rheum Dis* 1987;46:569-572.
13. Lemberskiy G, Novikov DS, Fieremans E. Artifact correction based on diffusion coefficient. *Int Soc Magn Reson Med* 2014;2595.
14. Steidle G, Schick F. Addressing spontaneous signal voids in repetitive single-shot DWI of musculature: Spatial and temporal patterns in the calves of healthy volunteers and consideration of unintended muscle activities as underlying mechanism. *NMR Biomed* 2015;28(7):801-810.
15. Szevenyi NM, Bydder G. Fasciculation MR imaging (faMRI) of the lower leg. *Int Soc Magn Reson Med* 2016;4258.
16. Whittaker RG, Porcari P, Braz L, Williams TL, Schofield IS, Blamire AM. Functional magnetic resonance imaging of human motor unit fasciculation in amyotrophic lateral sclerosis. *Ann Neurol* 2019;85(3):455-459.
17. Baliyan V, Das CJ, Sharma R, Gupta AK. Diffusion weighted imaging: Technique and applications. *World J Radiol* 2016;8(9):785-798.
18. Schwartz M, Steidle G, Martirosian P, et al. Estimation of the sensitivity characteristics and detection capability of diffusion-weighted MR sequences in imaging spontaneous mechanical activity in musculature. *Int Soc Magn Reson Med* 2017;5005.
19. Schwartz M, Steidle G, Martirosian P, et al. Spontaneous mechanical and electrical activities of human calf musculature at rest assessed by repetitive single-shot diffusion-weighted MRI and simultaneous surface electromyography. *Magn Reson Med* 2018;79(5):2784-2794.
20. Marty B, Baudin PY, Reyngoudt H, et al. Simultaneous muscle water T2 and fat fraction mapping using transverse relaxometry with stimulated echo compensation. *NMR Biomed* 2016;29(4):431-443.
21. Schwartz M, Martirosian P, Yang B, Schick F. A surface electromyography-driven magnetic resonance sequence controller for real-time myoelectric triggered imaging. *Annu Int Conf IEEE Eng Med Biol Soc* 2018;1356-1359.
22. Heskamp L, Birkbeck MG, Whittaker RG, Schofield IS, Blamire AM. The muscle twitch profile assessed with motor unit magnetic resonance imaging. *NMR Biomed* 2021;34(3):e4466.
23. Wymer DT, Patel KP, Burke WF, Bhatia VK. Phase-contrast MRI: Physics, techniques, and clinical applications. *Radiographics* 2020;40(1):122-140.
24. Shefner JM, al-Chalabi A, Baker MR, et al. A proposal for new diagnostic criteria for ALS. *Clin Neurophysiol* 2020;131(8):1975-1978.
25. Schwartz M, Martirosian P, Steidle G, et al. Volumetric assessment of spontaneous mechanical activities by simultaneous multi-slice MRI techniques with correlation to muscle fiber orientation. *NMR Biomed* 2018;31(11):e3959.
26. Schwartz M, Yang B, Schick F. Classification-guided Neural Network-based Correction of Magnetic Resonance-related Gradient Artifact Residuals in Simultaneously Recorded Surface Electromyography. In: *2022 44th Annual International Conference of the IEEE Engineering in Medicine & Biology Society (EMBC); 2022* 3632-3635.
27. Veraart J, Novikov DS, Christiaens D, Ades-aron B, Sijbers J, Fieremans E. Denoising of diffusion MRI using random matrix theory. *Neuroimage* 2016;142:394-406.
28. Heskamp L, Birkbeck M, Hall J, et al. Whole-body fasciculation detection in amyotrophic lateral sclerosis (ALS) using motor unit MRI (MUMRI). *Int Soc Magn Reson Med* 2022;S72-S73.
29. Schwartz M, Martirosian P, Steidle G, et al. Measuring spontaneous muscular activities in neuromuscular disease: Preliminary results. *Int Soc Magn Reson Med* 2020;2719.
30. Schwartz M, Steidle G, Martirosian P, et al. Improved spontaneous activity maps of resting skeletal musculature by surface EMG-based contraction pattern classification. *Int Soc Magn Reson Med* 2018;1405.
31. Otto L. *Quantitative MRI as a biomarker in spinal muscular atrophy*. Netherlands: Utrecht University; 2022.
32. Birkbeck MG, Heskamp L, Schofield IS, Blamire AM, Whittaker RG. Non-invasive imaging of single human motor units. *Clin Neurophysiol* 2020;131(6):1399-1406.
33. Heskamp L, Miller AR, Birkbeck MG, et al. In vivo 3D imaging of human motor units in upper and lower limb muscles. *Clin Neurophysiol* 2022;141:91-100.
34. Garnett RA, O'Donovan MJ, Stephens JA, Taylor A. Motor unit organization of human medial gastrocnemius. *J Physiol* 1979;287:33-43.
35. Stålberg E, Dioszeghy P. Scanning EMG in normal muscle and in neuromuscular disorders. *Electroencephalogr Clin Neurophysiol* 1991;81(6):403-416.
36. Feinstein B, Lindegård B, Nyman E, Wohlfart G. Morphologic studies of motor units in normal human muscles. *Cells Tissues Organs* 1955;23(2):127-142.
37. Christensen E. Topography of terminal motor innervation in striated muscles from stillborn infants. *Am J Phys Med* 1959;38(2):65-78.
38. Buchthal F, Schmalbruch H. Motor unit of mammalian muscle. *Physiol Rev* 1980;60(1):90-142.

39. Monti RJ, Roy RR, Edgerton VR. Role of motor unit structure in defining function. *Muscle Nerve* 2001;24(7):848-866.
40. de Carvalho M, Barkhaus PE, Nandedkar SD, Swash M. Motor unit number estimation (MUNE): Where are we now? *Clin Neurophysiol* 2018;129(8):1507-1516.
41. Sanchez GN, Sinha S, Liske H, et al. In vivo imaging of human sarcomere twitch dynamics in individual motor units. *Neuron* 2015;88(6):1109-1120.
42. Leitch M, Macefield VG. Comparison of contractile responses of single human motor units in the toe extensors during unloaded and loaded isotonic and isometric conditions. *J Neurophysiol* 2015;114(2):1083-1089.
43. Birkbeck MG, Heskamp L, Schofield IS, et al. Whole muscle and single motor unit twitch profiles in a healthy adult cohort assessed with phase contrast motor unit MRI (PC-MUMRI). *J Magn Reson Imaging* 2023;1-13. <https://doi.org/10.1002/jmri.29028>
44. Bergquist AJ, Clair JM, Collins DF. Motor unit recruitment when neuromuscular electrical stimulation is applied over a nerve trunk compared with a muscle belly: Triceps surae. *J Appl Physiol* 2011;110(3):627-637.
45. Birkbeck M, Heskamp L, Schofield IS, et al. Spontaneous motor unit activity in a healthy ageing population measured using motor unit MRI (MUMRI). *Int Soc Magn Reson Med* 2022;1027.
46. Goedee HS, Sleutjes BTHM, Bakers JNE, Kruitthof WJ, Kruitwagen-van Reenen ET, van der Pol WL. Electrophysiology of fatigue in chronic inflammatory demyelinating polyneuropathy: Can it be useful? *Clin Neurophysiol* 2020;131(12):2912-2914.
47. Barth M, Breuer F, Koopmans PJ, Norris DG, Poser BA. Simultaneous multislice (SMS) imaging techniques. *Magn Reson Med* 2016;75(1):63-81.